

Detection and Characterization of Rapidly Equilibrating Glycosylation Reaction Intermediates Using Exchange NMR

Frank F. J. de Kleijne‡, Floor ter Braak‡, Dimitrios Piperoudis, Peter H. Moons, Sam J. Moons, Hidde Elferink, Paul B. White* and Thomas J. Boltje*

Radboud University, Institute for Molecules and Materials (IMM), Synthetic Organic Chemistry, 6525 AJ, Nijmegen, The Netherlands

‡ These authors contributed equally

* Corresponding authors

Email: Paul.White@ru.nl, Thomas.Boltje@ru.nl

Abstract: The stereoselective introduction of glycosidic bonds (glycosylation) is one of the main challenges in the chemical synthesis of carbohydrates. Glycosylation reaction mechanisms are difficult to control because in many cases the exact reactive species driving product formation cannot be detected and the product outcome cannot be explained by the primary reaction intermediate observed. In these cases, reactions are expected to take place *via* other low-abundance reaction intermediates that are in rapid equilibrium with the primary reaction intermediate *via* a Curtin-Hammett scenario. Despite this principle being well-known in organic synthesis, mechanistic studies investigating this model in glycosylation reactions are complicated by the challenge of detecting the extremely short-lived reactive species responsible for product formation. Herein, we report the utilization of the chemical equilibrium between low abundance reaction intermediates and the stable, readily observed α -glycosyl triflate intermediate in order to infer the structure of the former species by employing exchange NMR. Using this technique, we enabled the detection of reaction intermediates such as β -glycosyl triflates and glycosyl dioxanium ions. This demonstrates the power of exchange NMR to unravel reaction mechanisms as we aim to build a catalogue of kinetic parameters allowing for the understanding and the eventual prediction of glycosylation reactions.

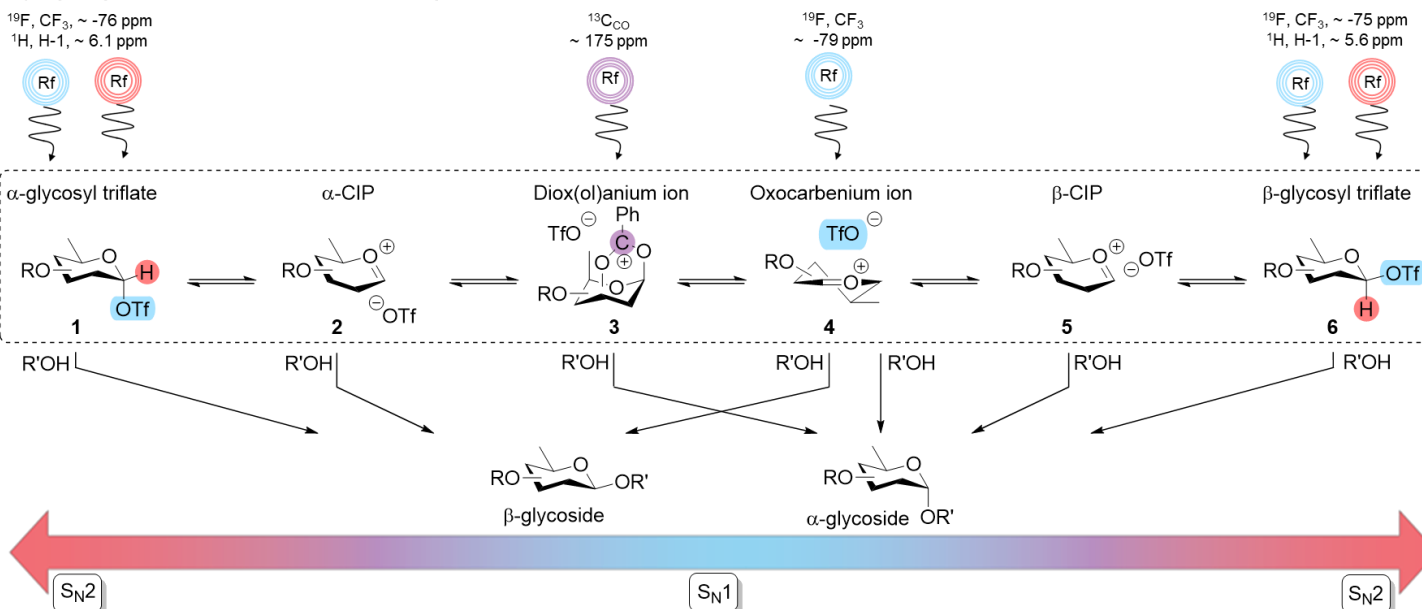
Introduction: The stereoselective introduction of glycosidic bonds (glycosylation) is one of the main challenges in the chemical synthesis of carbohydrates. In a chemical glycosylation reaction, an electrophile (the glycosyl donor) is activated by a chemical promotor and reacts with a nucleophile (the glycosyl acceptor). The nucleophile can add to the α - or β -face of reactive intermediates thereby leading to the formation of α - or β -diastereoisomers, respectively. Controlling the diastereoselectivity of glycosylation reactions can be achieved by the application of two main strategies.

First, a stereodirecting group, present on the donor molecule, can be employed to stabilize the glycosyl cation formed upon activation. An example of this principle is neighboring group participation (NGP) of an acyl group at the C-2 position affording a bicyclic dioxolanium ion intermediate **3** that reacts in a stereospecific manner with a glycosyl acceptor to afford a 1,2-*trans* product (Figure 1A).¹⁻⁴ Extension of this principle to acyl functionalities positioned on the C-3, C-4 or C-6 hydroxyl groups *via* NGP has also been suggested to direct the stereoselectivity of glycosylation reactions. However, whether selectivity can be attributed to NGP of the acyl group or other stereoelectronic effects is a subject of much debate.⁴⁻¹⁹ The second main strategy utilizes glycosyl donors that contain protecting groups that are less capable of neighboring group participation e.g. benzyl ethers. In this case the glycosyl cation is trapped by the promotor system counterion or a solvent additive to afford *quasi* stable intermediates that can be displaced in an S_N2 -like reaction pathway to afford a glycosylation product.²⁰⁻²² Most modern promotor systems give rise to the formation of glycosyl triflates and since these covalent adducts can exist in the α - (**1**) or β -form (**6**), reactions proceeding *via* these intermediates can in principle form the β - or α -product *via* an S_N2 -like reaction pathway, respectively.^{22,23} The nucleophilic displacement of α -glycosyl triflates **1** is likely to take place *via* an intermediate α -contact ion pair (CIP) **2** which maintains its stereochemical memory to form the β -product.²⁴ Full dissociation of the triflate would lead to the solvent separated ion pair (SSIP) **4**, which can afford glycosylation

products *via* an S_N1 -like pathway.²⁵⁻²⁷ The conformation of monosaccharide derived SSIPs is dictated by the relative stereochemistry of its substituents¹⁰ and is a crucial determinant of their stereoselectivity in glycosylation reactions.²⁵ Finally, β -glycosyl triflate CIP **5** and its corresponding covalent adduct **6** can form during glycosylation reactions from the SSIP or S_N2 -like displacement of the α -glycosyl triflate **1** by another triflate anion.²⁰ β -glycosyl triflates (on D-sugars) are not stabilized by the anomeric effect and hence less stable and more reactive. Since glycosylation reactions take place in a mechanistic continuum between these S_N1 - and S_N2 -like reaction pathways they are difficult to predict and control and very sensitive to parameters such as solvent^{28,29}, type of monosaccharide,^{17,30} strength of the nucleophile³¹ and reaction temperature.^{32,33}

To address this challenge, the characterization of reaction intermediates that drive product formation in glycosylation reactions is required. Glycosylation reaction intermediates can be characterized by employing Nuclear Magnetic Resonance (NMR) spectroscopy, and Infra-Red-Ion-Spectroscopy (IRIS), for example.^{26,34,35} These techniques have allowed for the characterization of intermediates such as glycosyl triflates^{22,23,34}, dioxolanium ions^{18,36,37}, dioxanium ions¹⁷ and even oxocarbenium ions.^{25,26,36,38} However, IRIS is performed in the gas-phase and the structure of reaction intermediates under these conditions may not always be relevant to those formed in solution. While NMR can be used to detect reaction intermediates in solution under relevant reaction conditions, the observation of a reaction intermediate does not automatically mean it is a reactive intermediate and hence relevant to product formation. In many cases the exact reactive species driving product formation remain unknown as the product outcome cannot be explained by the primary reaction intermediate observed. In these cases, reactions are expected to take place *via* other low-abundance reaction intermediates that are in rapid

A) Glycosylation reaction intermediates and products



B) Glycosyl donor investigated in this study

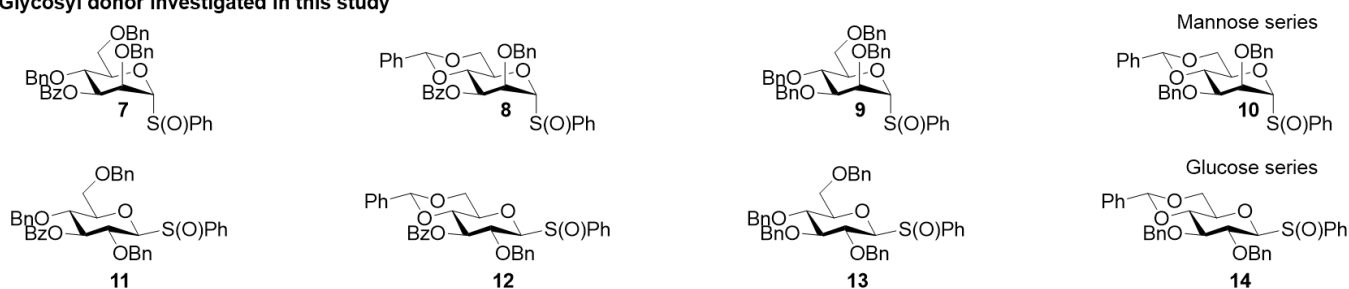


Figure 1: A) Glycosylation reaction intermediates and their characteristic resonances monitored by exchange NMR B) Glycosyl donors used in this study.

equilibrium with the primary reaction intermediate *via* a Curtin-Hammett scenario (Figure 1).^{20,39} Therefore, the stereochemical outcome of the reaction does not necessarily depend on the population of the intermediate leading to a given product but rather the overall barrier height when the barrier to intermediate interconversion is lower than the irreversible product-forming step.²⁰ Despite this principle being well-known in organic synthesis, mechanistic studies investigating this model in glycosylation reactions are complicated by the challenge of detecting the extremely short-lived reactive species responsible for product formation. The low abundance and short lifetime of these intermediates, such as **2-6**, complicate their characterization as they readily equilibrate back to form the more stable, readily observable but non-reactive α-glycosyl triflate intermediate **1**. We have utilized the chemical equilibrium between low abundance reaction intermediates and the stable, readily observed α-glycosyl triflate intermediate in order to infer the structure of the former species.¹⁷ Using chemical exchange saturation transfer (CEST) NMR we demonstrated that high-energy or “invisible” mannosyl dioxanium ions, which are formed by intramolecular stabilization of a C-3 ester, are in chemical exchange with the highly-populated α-glycosyl triflate intermediate.¹⁷

Herein, we report the application of this principle to detect the presence of other virtually undetectable high energy reaction intermediates relevant to product formation, such as β-triflates and dioxanium ions formed by internal stabilization. We characterized the reactive intermediates for a systematic set of eight frequently used glycosyl donors **7-14** (Figure 1B). Not only the presence of

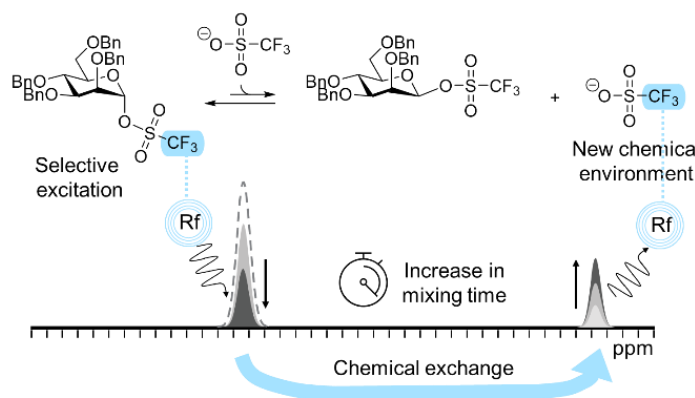
reactive intermediates but also their exchange kinetics were measured, thereby providing valuable quantitative data to elucidate the formation mechanism of the reactive intermediates. We report an integrated exchange NMR workflow to measure the reactivity of α-glycosyl triflates by monitoring the dissociation of the triflate ion using ¹⁹F exchange NMR spectroscopy (EXSY NMR). In addition, we established the mechanism of triflate dissociation with the same technique. A clear difference between mannose and glucose monosaccharides was observed in their triflate dissociation kinetics and mechanism. Mannosides were able to form dioxanium ions **7_d** and **8_d** *via* the participation of a C-3 acyl group whereas their glucoside counterparts were not and formed β-glycosyl triflates **11_{βOTf}**-**14_{βOTf}** instead. We were able to indirectly detect the presence of these low-population intermediates *via* their chemical equilibrium with the observable α-glycosyl triflate using ¹³C CEST, ¹H CEST, and ¹⁹F CEST NMR. Finally we were also able to characterize selected examples of the dioxanium ion and β-glycosyl triflate using more classical NMR techniques to unequivocally establish their structure. These results demonstrate the power of chemical exchange NMR to detect fleeting reaction intermediates to build a catalogue of kinetic parameters which allows for the understanding and ultimately prediction of glycosylation reactions. We expect this technique to be applicable to various other types of glycosylation reaction intermediates such as additives and solvents commonly used in glycosylation reactions, both of which tend to be rich in NMR-active nuclei that are sensitive to changes in chemical environment. Finally, the application of the workflow laid out herein should be applicable to other types of reaction that are under Curtin-Hammett control.

Results and Discussion

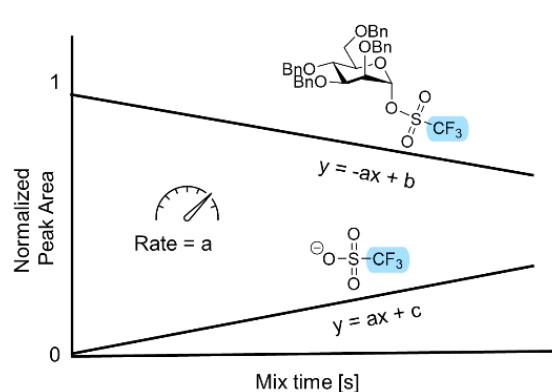
We started by investigating the stability and reactivity of glycosyl triflates derived from **7-14** to assess their likelihood of acting as reactive intermediates in glycosylation reactions. Previous experiments have investigated the decomposition temperature of glycosyl triflates as a measure of their stability/reactivity. While indicative of their thermal stability, such metrics do not necessarily speak to their relevance in product formation during a glycosylation event.⁴⁰ In addition, ¹H EXSY NMR has been used to monitor the interconversion of α - and β -glycosyl triflates²³ and mesylates⁴¹ providing kinetics of their interconversion. However, a major limitation of ¹H EXSY is that it requires both interconverting species to be visible in 1D NMR. This means that for the vast majority of glycosyl donors, intermediate exchange kinetics cannot be recorded due to the low populated state of the highly reactive β -triflate intermediates. Another means of measuring α -glycosyl triflate stability and reactivity is by observing the kinetics of triflate dissociation in the absence of an acceptor using ¹⁹F EXSY NMR. Since both the α -glycosyl triflate and unbound triflate anion, which results from the activation step (*vide infra*), are always observed and exist as strong signals, we reasoned that if we could observe the interconversion between bound- and free-triflate then that would indicate the presence of an unobserved intermediate. Hence, we started by investigating the stability/reactivity of eight glycosyl triflates derived from **7-14** using ¹⁹F EXSY NMR, which revealed all eight species underwent triflate exchange. The preparation of the thioglycoside precursors used to generate glycosyl triflates **7_{OTf}-14_{OTf}** is described in the supporting info (SI page S12-S31). The glycosyl triflates were generated by activating

the corresponding glycosyl sulfoxide donor with triflic anhydride (Tf₂O) in the presence of the non-nucleophilic base 2,4,6-*tert*-butyl-pyrimidine (TTBP) in CD₂Cl₂ at -80 °C inside an NMR tube (please see page S7-S10).⁴² Clean formation of glycosyl triflates (**7_{OTf}-14_{OTf}**) was observed in all cases (Figure S4-11). Dissociation of the anomeric triflate to unbound triflate could be monitored using selective ¹⁹F EXSY NMR (SI page S2-S4, S7). Magnetization of the selectively-excited CF₃ resonance of the α -glycosyl triflate is transferred to the unbound triflate ion upon triflate dissociation during the ZZ-exchange mix time (Figure 2A). By plotting the mix time vs the extent of magnetization transfer, the rate of triflate dissociation was measured, which we propose is an indicator of α -glycosyl triflate stability (Figure 2B). In order to be compare measurements across different sugars and samples while also taking into account multiple mechanisms, the reported rates in Figure 2 are normalized by dividing the measured rate by the initial α -triflate concentration (see SI page S2-4). By subsequently repeating this process at different temperatures, the normalized rate of triflate dissociation as a function of temperature was established (Figure 2C, Figure S49-S85). A few important considerations are needed to ensure reliable kinetic data to emerge from the ¹⁹F EXSY experiments. First, the exchanging system needs to be in the slow-exchange regime which is defined by the rate of exchange being much lower than the frequency difference between the interconverting species ($k_1 + k_{-1} \ll \Delta(\omega_{A-B})$). Secondly, to reduce the complexity of modelling the kinetics, we chose to measure initial rates for the exchange processes, which puts a rough limit to the maximum normalized rate of $\sim 100 \text{ s}^{-1}$ (10% conversion at 1 ms mix time). Furthermore, the slowest measurable

A) ¹⁹F EXSY NMR on Glycosyl triflates



B) Triflate dissociation rate using ¹⁹F EXSY data



C) Rate of triflate dissociation from α -glycosyl triflates **7_{OTf} - 14_{OTf}** determined by ¹⁹F EXSY at different temperatures

Temp	7_{OTf}	8_{OTf}	9_{OTf}	10_{OTf}	11_{OTf}	12_{OTf}	13_{OTf}	14_{OTf}
-80 °C	0.29 ± 0.01	Too slow	-	-	-	-	-	-
-70 °C	1.3 ± 0.02	0.11 ± 0.004	Too slow	-	Too slow	-	Too slow	-
-60 °C	4.3 ± 0.05	0.25 ± 0.001	0.15 ± 0.004	-	0.088 ± 0.005	-	0.28 ± 0.004	-
-50 °C	10 ± 0.3	0.68 ± 0.01	0.36 ± 0.004	-	0.18 ± 0.005	Too slow	0.56 ± 0.01	Too slow
-40 °C	Decomposed	1.8 ± 0.03	1.1 ± 0.04	0.11 ± 0.007	0.63 ± 0.006	0.10 ± 0.004	2.4 ± 0.03	0.15 ± 0.002
-30 °C	-	4.6 ± 0.08	Decomposed	0.27 ± 0.009	Decomposed	0.20 ± 0.003	Decomposed	0.35 ± 0.003
-20 °C	-	13 ± 0.1	-	0.65 ± 0.03	-	0.65 ± 0.004	-	1.4 ± 0.01
-10 °C	-	Decomposed	-	Decomposed	-	2.4 ± 0.02	-	5.6 ± 0.05
0 °C	-	-	-	-	-	Decomposed	-	Decomposed

Rate (10⁻⁴) [s⁻¹]

Figure 2: A) Working principle behind ¹⁹F EXSY NMR to monitor triflate dissociation. The α -glycosyl triflate is selectively excited and then observed over time transforming into free triflate. B) Determination of the initial rate of triflate dissociation. C) Summary of normalized triflate dissociation rates (s⁻¹) across the studied glycoside series as a function of temperature.

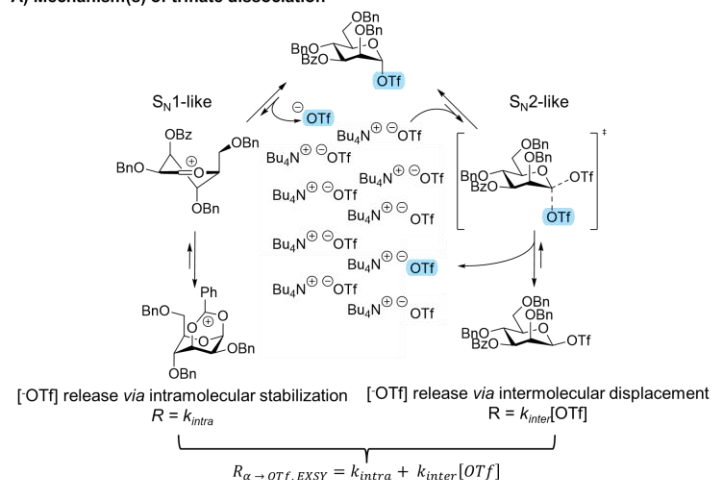
rate is related to the T_1 of the observed nucleus. Hence, the T_1 of the nuclei, and more importantly, the difference in T_1 between the resonances of interest, should be taken into consideration when setting the maximum mix time. For ^{19}F , the T_1 s of the α -triflate $10_{\alpha\text{OTf}}$ and soluble triflate salt were measured at -80°C where exchange was frozen and found to be roughly identical (0.31 s and 0.42 s, respectively, Figure S48). This allowed us to make the approximation that T_1 losses for each were roughly equivalent and hence could be ignored thereby allowing us to extend our mix range past T_1 . Therefore, we were able to measure normalized rates accurately down to $\sim 0.1\text{ s}^{-1}$. Third, the population of the α -glycosyl triflate and free triflate should not significantly change from the beginning to the end of experiment. Therefore, once thermal decomposition begins to take hold, these experiments become unreliable and thus limits the upper limit of the temperature window.

Keeping in mind these considerations, the rates of triflate dissociation from the parent α -glycosyl triflates $7_{\alpha\text{OTf}}$ – $14_{\alpha\text{OTf}}$ at various temperatures were obtained (Figure 2C). Interestingly, clear differences in triflate dissociation were observed that related to the relative stereochemistry of the monosaccharide (mannose vs glucose) and the protecting group pattern. Mannosyl triflate $7_{\alpha\text{OTf}}$ and $8_{\alpha\text{OTf}}$ carrying a single benzoate ester at C-3 showed the fastest triflate dissociation. Interestingly, the benzylidene protected mannosyl analogue $8_{\alpha\text{OTf}}$ carrying a C-3 benzoate ester was second fastest in the mannose series. Benzylidene protected monosaccharides are typically classified as disarmed due to the torsional^{43,44} and electronic effects⁴⁵ induced by the fused benzylidene ring system.⁴⁰ Indeed triflate dissociation for $8_{\alpha\text{OTf}}$ was slower than the corresponding benzylated analogue $7_{\alpha\text{OTf}}$ but still faster than the fully benzylated compound $9_{\alpha\text{OTf}}$. This suggests a role of the C-3 ester in driving triflate release, overpowering the disarming effect induced by the benzylidene. This is confirmed by the fact that the benzylidene protected mannosyl triflate containing benzyl ethers at C-2 and C-3 was slowest in the mannose series in triflate dissociation. Interestingly, the opposite trend was observed in the glucose series. The difference in rate for the C-3 benzoyl $11_{\alpha\text{OTf}}$ and $12_{\alpha\text{OTf}}$ vs C-3 benzyl $13_{\alpha\text{OTf}}$ and $14_{\alpha\text{OTf}}$ analogues was much smaller with the former being slower, particularly at higher temperature. As expected, the benzylidene protected analogues $12_{\alpha\text{OTf}}$ and $14_{\alpha\text{OTf}}$ showed slower triflate dissociation compared to their benzylated counterparts $11_{\alpha\text{OTf}}$ and $13_{\alpha\text{OTf}}$. Overall these results indicate that the presence of a benzylidene acetal compared to the benzylated analogue slows down triflate dissociation for both the mannose and glucose series. However, the introduction of a C-3 benzoyl group speeds up triflate dissociation in the mannose series and slows down triflate release in the glucose series.

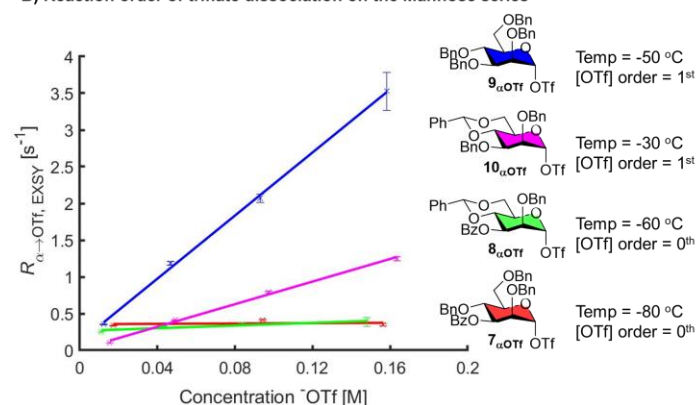
The striking differences in triflate dissociation rates are likely the result of a different mechanism of triflate dissociation, but these cannot be established from the rates alone. Hence, we set out to investigate the mechanism of triflate dissociation of $7_{\alpha\text{OTf}}$ – $14_{\alpha\text{OTf}}$ to explain their dissociation rate differences. We foresee three main equilibria that would lead to the dissociation of the triflate anion (Figure 3A). First, dissociation of the triflate anion could lead to a SSIP. Secondly, NGP of the C-3 acyl substituent present in molecules $7_{\alpha\text{OTf}}$ – $8_{\alpha\text{OTf}}$ could take place to form a dioxanium ion with or without an intermediary SSIP. Third, a triflate anion could displace the α -glycosyl triflate in an $\text{S}_{\text{N}}2$ -like manner to form the corresponding β -triflate. To dissect the mechanism(s) responsible for triflate

dissociation we investigated the rate of this process as a function of the triflate anion concentration. The rate of triflate dissociation from the α -glycosyl triflate *via* SSIP and/or dioxanium ion formation should be insensitive to the triflate concentration. The rate of triflate dissociation from the α -glycosyl triflate *via* $\text{S}_{\text{N}}2$ -like displacement to form the corresponding β -glycosyl triflate should be first order with respect to the triflate concentration. In case both processes operate simultaneously, the sum of the rates would constitute the overall rate of triflate dissociation (Figure 3A). The temperature for the study was chosen so that if a first-order dependence was found, it would not move the kinetics outside the window for EXSY and at the same time being suitably fast enough to study if no dependence was discovered. Next, using the aforementioned ^{19}F EXSY scheme, we measured the triflate dissociation as a function of triflate concentration at a single temperature by the addition of tetrabutylammonium triflate (TBAT).

A) Mechanism(s) of triflate dissociation



B) Reaction order of triflate dissociation on the Mannose series



C) Reaction order of triflate dissociation on the Glucose series

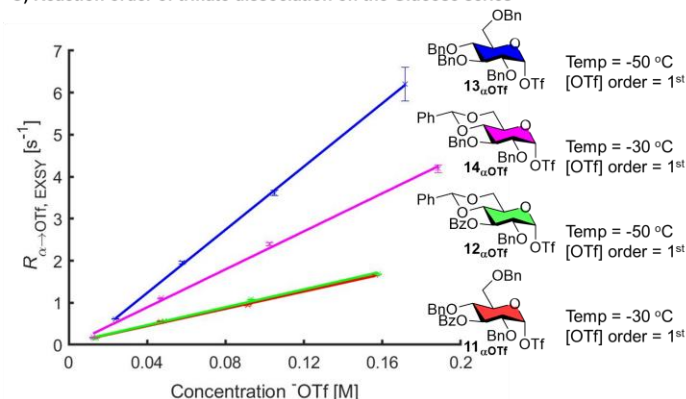


Figure 3: A) $\text{S}_{\text{N}}1$ and $\text{S}_{\text{N}}2$ -like triflate dissociation mechanisms. B) Reaction order determination for triflate dissociation in the Mannose series and C) Glucose series.

To this end, the triflate concentration was increased in steps by taking the sample out of the probe and adding 1 M TBAT solution in dry CD_2Cl_2 at -80°C to approximately double the triflate concentration in each step. The exact triflate concentration was determined by comparison to the trimethyl(4-(trifluoromethyl)-phenyl)silane internal standard. The results are plotted in Figure 3B-C and show a clear dichotomy in the mechanism of triflate dissociation, consistent with the observed temperature dependent rate differences listed in Figure 2C. C-3 Benzoyl-containing mannosides **7** $_{\alpha\text{OTf}}$ -**8** $_{\alpha\text{OTf}}$ showed a 0th-order rate dependence with respect to the triflate concentration. These results indicate that internal stabilization of the C-3 benzoyl, which forms the dioxanium ion, drives triflate dissociation. In contrast, all glucosides (**11** $_{\alpha\text{OTf}}$ -**14** $_{\alpha\text{OTf}}$) and both mannosides lacking the C-3 benzoyl group (**9** $_{\alpha\text{OTf}}$ -**10** $_{\alpha\text{OTf}}$) show a 1st order triflate concentration dependence for the rate of triflate dissociation (Figure 3B-C). These data suggest that these molecules likely undergo a $\text{S}_{\text{N}}2$ -like triflate displacement to form the β -glycosyl triflate. Furthermore, this demonstrates that internal stabilization by the C-3 acyl group is reserved to the mannose donors while the glucose counterparts likely form β -glycosyl triflates.

The above ^{19}F EXSY studies established the rates of triflate dissociation as well as provided evidence for its mechanism but does not confirm the presence of the intermediates proposed in such mechanisms. Since EXSY can only be applied if both intermediates are readily visible in 1D NMR, it cannot be used to study the expected dioxanium ions and/or β -glycosyl triflate intermediates due to their low population at equilibrium. Hence, to solve this challenge, a different technique is needed. As mentioned above, chemical exchange saturation transfer (CEST) NMR is well suited to detect very low population “invisible” reaction intermediates that are in a chemical equilibrium with a visible reaction intermediate. This technique, originally developed as a contrast approach in MRI,⁴⁶ has been applied by Gschwind *et al.* to detect iminium ions and by us to detect mannosyl dioxanium ions, for example.^{17,47} The main advantage of CEST NMR is that no prior information about the chemical shift of the low-populated intermediate resonance is required since the experiment scans a given frequency domain by incrementing the saturation offset frequency while monitoring the transfer of saturation to the main observable species *via* chemical exchange (Figure 4A). Furthermore, by varying saturation times the interconversion kinetics for these intermediates can be quantified.⁴⁸ The limitations of CEST are similar to EXSY: the chemical exchange is slow on the NMR timescale ($k_1 + k_{-1} \ll \Delta(\omega_{\text{A-B}})$), and the detection window is defined by a combination of relative population exchanging species and longitudinal relaxation rate (R_1).^{46,49} Since the dioxanium ions can only form from the C-3 benzoyl containing compounds **7-8** we investigated this set using ^{13}C CEST NMR. To this end, ^{13}C labelled substrates **7** $^{13\text{C}}$ and **8** $^{13\text{C}}$ were prepared to enable the sensitive detection of the carbonyl quaternary carbon (SI page S12-31). By incrementing the saturation offset frequency while monitoring the transfer of saturation to a reporter peak ($^{13}\text{C}=\text{O}$) on the main observable species (α -glycosyl triflate) *via* chemical exchange we investigated the detection of mannosyl and glucosyl dioxanium ion formation (Figure 4, Top, SI Figure S13-17). Apart from the use of a ^{13}C -labelled starting material, the CEST NMR experiments were performed under identical conditions as the EXSY experiments. As expected, the mannosyl triflate **7** $^{13\text{C}}_{\alpha\text{OTf}}$ showed saturation transfer at the chemical shift expected for the dioxanium ion ($\delta_{\text{C}} = 177$ ppm,

Figure 4A). In contrast, the mannosyl benzylidene derivative **8** $^{13\text{C}}_{\alpha\text{OTf}}$ did not (Figure 4B), even though the formation of a dioxanium ion was expected based on an observed 1st-order triflate dependence.

General activation scheme and graphical visualization of ^{13}C CEST

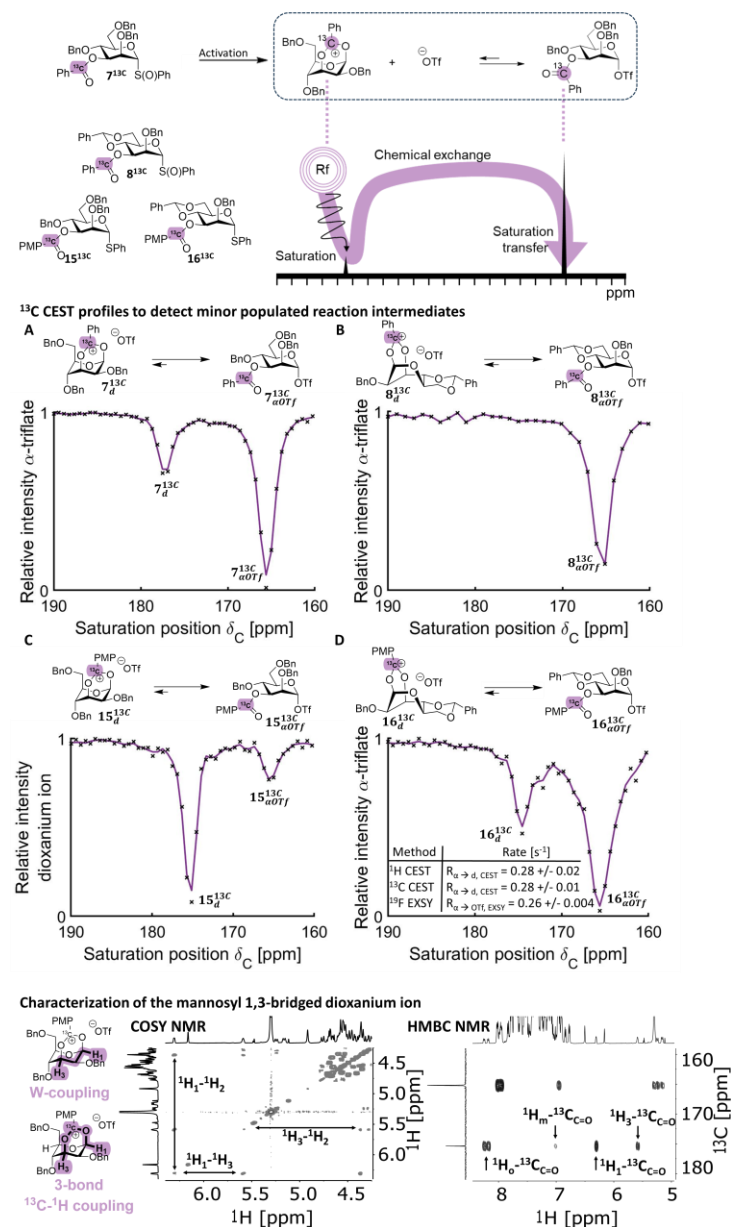


Figure 4: Top) Mechanism of ^{13}C CEST NMR to detect neighboring group participation. **A-D)** CEST profiles for ^{13}C -labelled C-3 acyl-protected mannosyl and glucosyl donors. **Bottom)** Characterization of mannosyl dioxanium ion using HMBC and COSY.

Due to the presence of the benzylidene, the molecule is less flexible and requires the formation of a tricyclic dioxanium ion which is likely much slower and less stable than the non-benzylidene derivative **7** $_{\text{d}}$. This may explain why CEST NMR was unable to pick up the dioxanium ion as the CEST NMR technique is limited by the population of the minor exchanging species and the rates of dioxanium ion formation and consumption ($k_{\alpha \rightarrow \text{d}}$ and $k_{\text{d} \rightarrow \alpha}$ respectively). If the population of the intermediate is well below 1% or the exchange has moved into the intermediate or fast regime ($k_{\alpha \rightarrow \text{d}} + k_{\text{d} \rightarrow \alpha} > \Delta\omega_{\text{d}\alpha}$), then the minor exchanging species cannot be detected. Due to the intrinsically high reactivity of a tricyclic dioxanium ion, it is likely that dioxanium ion consumption ($k_{\text{d} \rightarrow \alpha}$) is exceedingly fast, hence, limiting detection of the ion by ^{13}C CEST NMR. The corresponding glucose series (**11** $^{13\text{C}}$ and **12** $^{13\text{C}}$) did not show dioxanium ion formation *via* CEST (Figure S14 and S16), fully consistent with the 1st-order triflate dependence (Figure 3C). In

light of the conflicting CEST results with the triflate order in the case of mannosyl triflate **x**, we reasoned that we could be approaching the limitation of the CEST NMR viewing window outlined above. Therefore, we wanted to boost the observable population of the dioxanium ion by preparing the corresponding *p*-anisoyl derivatives **15**^{13C} and **16**^{13C} of the mannose series as the electron-donating methoxy group should increase the stability of the dioxanium ion and slow down the α -glycosyl triflate formation. Additionally, we performed the activation of **15**^{13C} and **16**^{13C} in the absence of TTBP to minimize the free triflate anion concentration in an effort to further boost the population of dioxanium ion.¹⁷ Under these conditions, saturation transfer of the dioxanium ion was observed in both cases (Figure 4C and D). For benzylidene derivative **16**^{13C}, it was now possible to detect the dioxanium ion with ^{13C} CEST NMR, which aligned with its 0th-order triflate dependence. Furthermore, mannosyl donor **15**^{13C} showed a much higher population (~45%) of dioxanium ion compared to benzoyl derivative **7**. Due to the very high population of dioxanium upon activating α donor **15**^{13C}, we were able to use the dioxanium ion signal as the reporter peak of the CEST NMR experiment in order to detect if there were additional intermediates in chemical exchange with it. Identical to the benzoyl-derivative, the α -glycosyl triflate was the only detectable species in chemical exchange with the dioxanium ion. Fortunately, due to the high population of ion **15**^{13C}_d, we could fully characterize it using ¹H-¹³C HMBC and ¹H-¹H COSY experiments (Figure 4, Bottom). We had previously reported the characterization of a similar 3-benzoyl-2,4,6-trimethylated mannosyl dioxanium ion but these results now demonstrate its formation with relevant protecting groups which are routinely used in oligosaccharide synthesis. Hence, although not directly observed, we expect the characteristic saturation transfer at 175 ppm for benzylidene derivative **16**^{13C} to correspond to the tricyclic mannosyl dioxanium ion **16**^{13C}_d. To further solidify this hypothesis we measured the triflate dissociation of **16**^{13C}_{OTf} with ¹⁹F EXSY and dioxanium ion formation using ¹H and ¹³C CEST NMR. The measured rate from these techniques were 0.28 ± 0.02 s⁻¹, 0.28 ± 0.01 s⁻¹ and 0.26 ± 0.004 s⁻¹, respectively, indicating that the processes for forming the dioxanium and dissociating the triflate group are clearly coupled (Figure 4D). From these results it is clear that mannoside **15**^{13C} and **16**^{13C} showed formation of the C-3 dioxanium ion, which is consistent with the α -selective glycosylation behaviour of **7** and **8** and the observation that their triflate dissociation rates are irrespective of the triflate anion concentration.

The C-3 acylated mannosides above are a privileged class of glycosides as all of the other cases (**9**_{OTf}-**14**_{OTf}) displayed a 1st-order triflate anion concentration dependence for triflate dissociation. These observations are consistent with an equilibrium between an α - and β -glycosyl triflate. β -glycosyl triflates are exceedingly difficult to detect and have only been observed in case of benzylidene-protected methylated glucose and allose donors using ¹³C labelled monosaccharides.²³ Only in case of the allose, a large enough population of β -glycosyl triflate was formed that allowed for the investigation of its exchange kinetics using ¹H EXSY.²³ Furthermore, an equatorial triflate not stabilized by the anomeric effect formed *via* a conformational ring flip was observed by Van der Marel and co-workers.⁵⁰ To the best of our knowledge, these two reports forms the summative collection of observed glycosyl triflates not stabilized by the anomeric effect. To enable the detection of unstable and very low populated β -glycosyl triflates we again applied CEST NMR but focused on the ¹H and ¹⁹F nuclei. For

¹H CEST NMR, the H-1 signal belonging to the α -glycosyl triflate was used as a reporter peak and the saturation offset frequency was scanned while monitoring saturation transfer to this peak (Figure 5, Top). Upon detection of a possible β -glycosyl triflate, saturation transfer from an upfield peak position (~5.5-5.7 ppm) would be expected to be observed. None of the mannoside donors displayed a chemical equilibrium with an upfield resonance with the exception of benzylidene derivative **10**, which we tentatively assigned as β -glycosyl triflate **10**_{OTf} (Figure 5A-H).

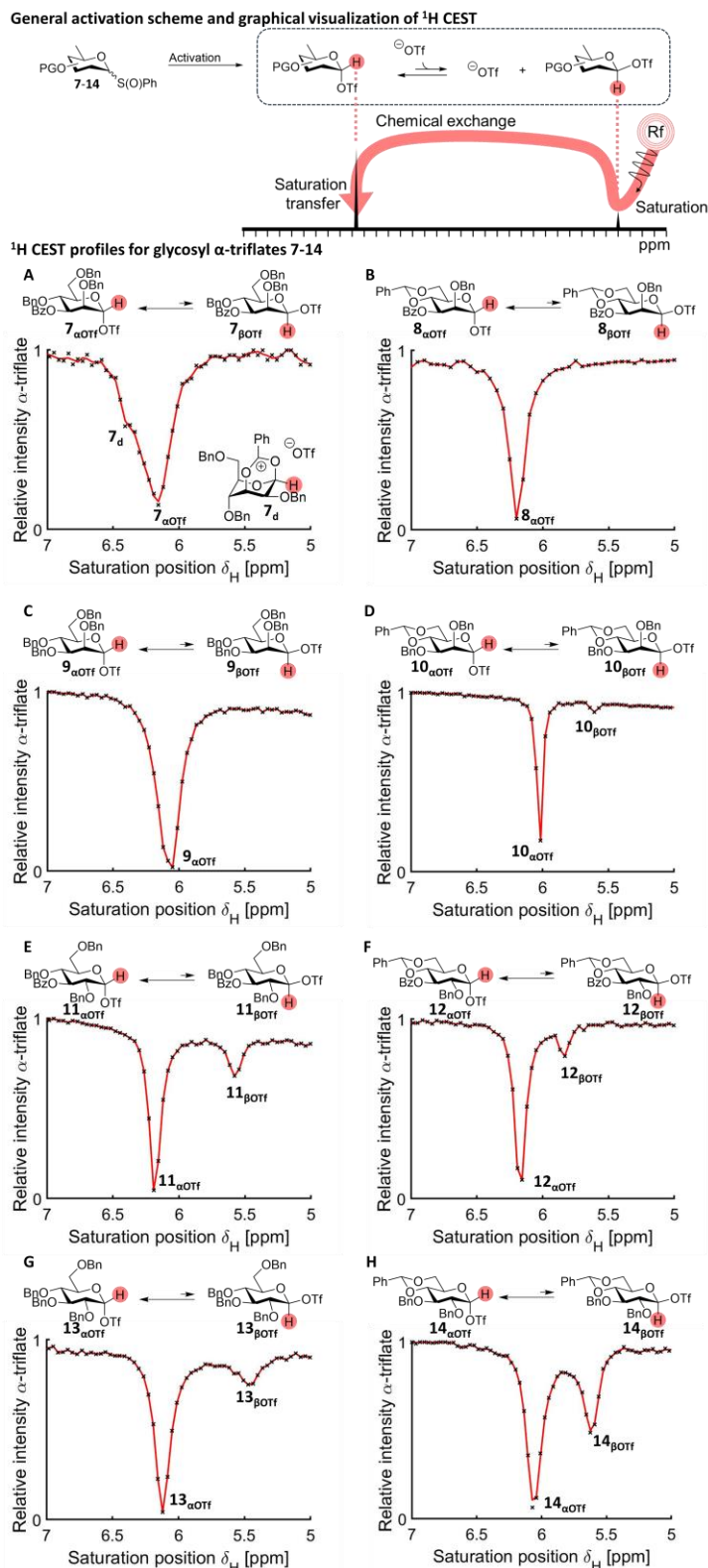


Figure 5: Top) Mechanism of ¹H CEST NMR to detect β -glycosyl triflates. **A-H)** ¹H CEST profiles for **7**_{OTf}-**14**_{OTf}.

These results are consistent with the triflate orders obtained for three of these compounds **7** and **8** (0th order, no β -glycosyl triflate detected) and **10** (1st order, β -glycosyl triflate detected). Only for

perbenzyl mannosyl donor **9**, we did not detect a β -glycosyl triflate even though its triflate dissociation rate is 1st order in triflate concentration. This could be due to a very low population of β -glycosyl triflate at equilibrium or the system has moved out of the slow-exchange regime in which case it would be difficult or impossible to detect with ¹H CEST NMR. In contrast, all of the glucose series donors (**11-14**) showed clear saturation transfer via an upfield peak that we presume is a β -glycosyl triflate. These results are fully consistent with their 1st order triflate dependence (Figure 3B-C). We validated these results by repeating β -glycosyl triflate detection using the ¹⁹F channel. For ¹⁹F CEST NMR, the CF₃ signal belonging to the α -glycosyl triflate ion was used as a reporter peak and the saturation offset frequency was scanned while monitoring saturation transfer to this peak (Figure S19-S26). As a consequence, all ¹⁹F CEST NMR spectra identify chemical exchange with the “free” triflate anion pool which can arise from either the α - or β -glycosyl triflate. The ¹⁹F CEST NMR results are fully consistent with those obtained from the ¹H CEST NMR experiments. For the mannose series, chemical exchange of the α -glycosyl triflate with the unbound triflate anion could be clearly observed via saturation transfer monitored from the α -glycosyl triflate at -75.9 ppm (Figure S22). Only for the benzylidene derivative **10** an additional saturation transfer from a presumed β -glycosyl triflate was observed at -75.0 ppm, similar to the ¹H CEST NMR. Moreover, in case of the glucose series, saturation transfer from β -glycosyl triflates could be detected in all cases using ¹⁹F CEST NMR as was the case for the corresponding ¹H experiments.

To obtain additional proof that the saturation transfer originates from exchange with a the β -glycosyl triflate, we set out to further characterize this low population species. From the glucose set, benzylidene derivative **14** displayed the clearest formation of this species and we thus investigated this molecule further. The only reported direct spectroscopic evidence of a β -glycosyl triflate was obtained for a very similar compound, 4,6-benzylidene-2,3-di-*O*-methyl glucosyl- β -triflate by Asensio and co-workers.²³ We prepared the corresponding benzyl protected compound with a C-1 ¹³C isotope label (**14**¹³C-1) in order to measure the ¹J_{C1-H1} and ³J_{H1-H2} coupling constants, which are indicative of the stereochemistry at C-1. Upon activation, this derivative formed a small (\approx 1%, SI, Figure S46) population of β -glucosyl triflate which could be characterized using a ¹H-¹³C HSQC NMR experiment where the ¹³C decoupler was not applied during the acquisition period (Figure 6). This is experiment serves as a simple method for measuring the ¹J_{CH} as well as allowing for long F2 acquisition times to obtain high-resolution peaks in the ¹H dimension suitable for measuring ¹H-¹H couplings. The ¹J_{C1-H1} coupling constant for the minor species was determined to be 175 Hz compared to 183 Hz for the corresponding α -derivative (Figure 6). This 8 Hz decrease in coupling constant is indicative of an axial H-1 found in β -configured molecules.⁵¹ Most importantly, the ³J_{H1-H2} coupling constant was measured to be 7.5 Hz, which is consistent with the axial-axial coupling expected for a β -glycosyl triflate intermediate. Lastly, the chemical shifts of C-1 and H-1 are also consistent with a glycosyl triflate species and the two ¹³C resonances at 106.4 ppm (α -triflate) and 104.3 ppm (β -triflate) as determined from the HSQC were shown to undergo chemical exchange via ¹³C CEST NMR (Figure S47).

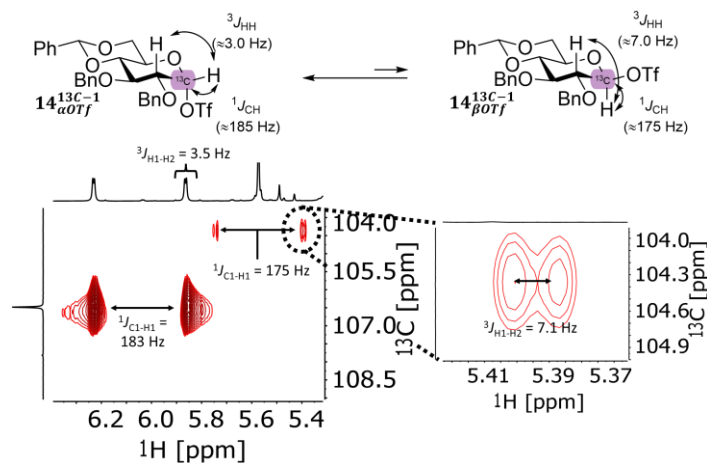


Figure 6: Characterization of β -glycosyl triflate **14** using HSQC without ¹³C decoupling in order to measure ¹J_{C1-H1} and ³J_{H1-H2}.

The systematic set of exchange NMR experiments described above allows for the development of a rationale for the reaction pathways leading to the stereoselective formation of glycosylation product(s) for each of the eight glycosyl donors **7-14** studied. For all eight examples, the main reaction intermediate formed after activation is the α -glycosyl triflate. A baseline of S_N2-like displacement pathway leading to the β -product can therefore be expected in all cases. The SSIPs involved in the reactions could not be detected due to their instability but for both the mannose^{10,25} and glucose²⁵ series are expected to react via their α -selective ⁴H₃ half-chair conformers. Additional pathways proceeding via C-3 participation and β -glycosyl triflate intermediate can also lead to α -selective product formation. The rate differences of reaction intermediate interconversion and the ensuing product forming step therefore dictate the stereospecific outcome as outlined by Lemieux and co-workers.²⁰ The stereoselectivity for all eight glycosyl donors **7-14** as a function of acceptor reactivity was investigated separately.¹⁸

Starting with the mannose series, C-3 benzoyl mannosyl donor **7** provides α -mannosides upon glycosylation.^{17,18} The corresponding α -glycosyl triflate **7**_{αOTf} is the main observable reaction intermediate but does not give direct access to the α -product via an S_N2-like pathway. Hence, glycosylation likely takes place via a rapidly equilibrating dioxanium ion **7**_d and/or β -glycosyl triflate **7**_{βOTf} which would afford the α -product. Dioxanium ion **7**_d was observed via CEST NMR while the β -glycosyl triflate was not nor was it expected to be based on its 0th-order triflate dependence. Therefore, we confidently propose that the reactive intermediate in this case is the dioxanium ion and that the system is under Curtin-Hammett control (Figure 7).

The corresponding C-3 benzoyl-4,6-benzylidene mannoside **8** shows a similar profile. The α -mannoside is formed upon glycosylation which cannot be explained via the observable α -glycosyl triflate intermediate.⁵² CEST NMR was unable to confirm the presence of dioxanium ion **8**_d or β -triflate **8**_{βOTf}. However, the rate of triflate dissociation from **8**_{αOTf} was independent of the triflate concentration pointing towards triflate dissociation via C-3 participation. By substituting the C-3 benzoyl for anisoyl in order to further stabilize the cation, the resulting dioxanium ion was detected for the first time. The existence of this intermediate has long been debated,^{5,6} and frequently omitted from consideration.^{5,14,52} However, the experiments support its existence as the chemical shift, triflate order and glycosylation stereoselectivity all support the existence of dioxanium ion **8**_d and its role as a product-forming intermediate (Figure 7).

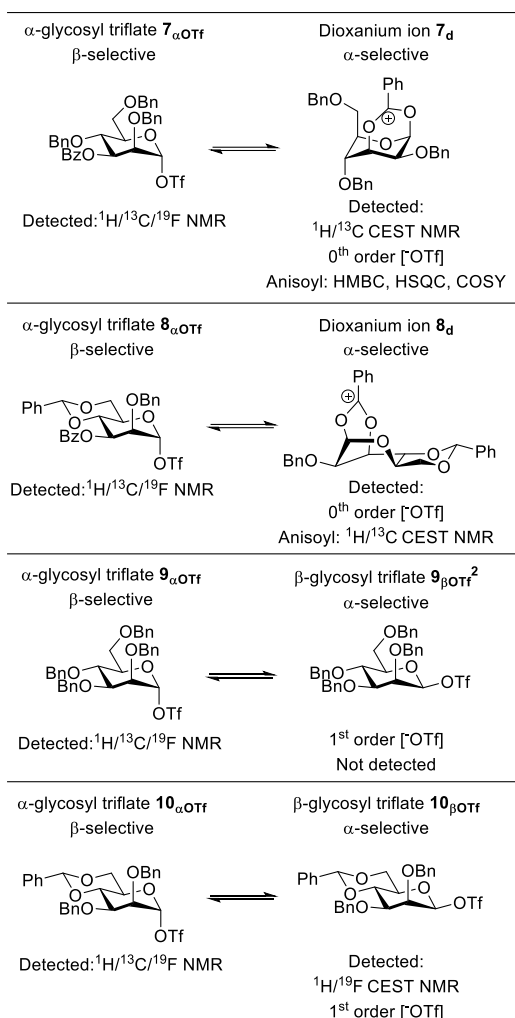


Figure 7: Spectroscopic summary of mannosyl intermediates.

Perbenzyl mannoside **9** is a much less selective glycosylation donor. The 1^{st} order of the triflate concentration on triflate dissociation support the formation of a β -glycosyl triflate although this species could not be detected *via* the exchange NMR experiments. We hypothesize that a dynamic equilibrium of α -, β -glycosyl triflates and possibly the SSIP is present leading to various product forming pathways and hence mixed stereoselectivity.

4,6-benzylidene mannoside **10** is known to provide β -products upon glycosylation.³⁹ This can be explained by an $\text{S}_{\text{N}}2$ -like displacement of the corresponding α -contact ion pair.²⁴ Hence, in this case, the main observed reaction intermediate is assigned as the reactive intermediate. Interestingly, CEST NMR did show the presence of an equilibrium with the β -triflate intermediate, which is consistent with its 1^{st} order triflate dependence. Interestingly, this equilibrium is not relevant for product formation with most nucleophiles and therefore represents a situation where the β -triflate is the less reactive species (Figure 7).

The glucose series showed very different stereoselectivity in glycosylations compared to the corresponding mannose series as noted earlier by Crich and co-workers.³⁰ In sharp contrast to the mannose series, no evidence for dioxanium ion formation by a C-3 acyl neighboring group in **11** and **12** was found (Figure 8). The origin of this striking difference was investigated further in a separate study. Both molecules form β -glycosyl triflates whereas the mannosides do not, but these lead to a lower α -selectivity than the dioxanium ions in the case of their mannose counterparts.¹⁸ Also the origin of this clear divergence was investigated further in a separate study.

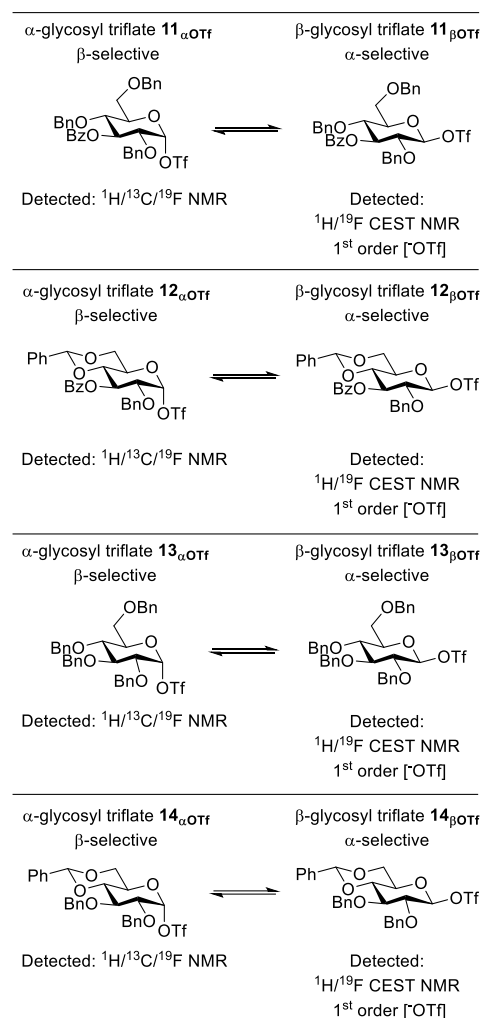


Figure 8: Spectroscopic summary of glucosyl intermediates.

A role for the SSIP, which is expected to adopt a 4H_3 halfchair conformer and drives the formation of α -product as reported by Codée and co-workers, cannot be excluded.²⁵ The simultaneous operation of multiple product forming pathways likely leads to a lower stereoselectivity in these cases. The two glucosides **13** and **14** lacking the C-3 benzoyl group show a similar, moderate stereoselectivity compared to their C-3 benzoyl counterparts (Figure 8).¹⁸ This underscores the lack of stereodirecting capability of the C-3 substituent in glucose.¹⁸ The benzylidene derivative **14** has been demonstrated to be α -selective in contrast to its mannose derivative.³⁰ Since **14** also clearly showed to be in equilibrium with the β -glycosyl triflate, we assign this as a major reactive intermediate driving α -product formation (Figure 8).

Conclusions

We were able to directly and indirectly detect the presence of low-population reaction intermediates *via* their chemical equilibrium with the readily observable α -glycosyl triflate for a collection of eight of gluco- and mannosides bearing either C-3 acyl or benzyl substituent. The stability of α -glycosyl triflates and their mechanism for dissociation could be readily measured using ^{19}F EXSY NMR. This allowed for their role in glycosylation reactions to be ascertained. Furthermore, equilibria with low-population intermediates such as dioxanium ions and β -glycosyl triflates could be detected using ^{13}C CEST, ^1H CEST, and ^{19}F CEST NMR. Finally, selected examples of the dioxanium ion and β -glycosyl triflate were characterized using classical NMR techniques to unequivocally establish their identity. The results provide the first mechanistic proof for the existence of mannosyl dioxanium ions and β -glucosyl triflates utilizing relevant protecting groups and under actual reaction conditions. These

observations allow for the rationalization of their observed α -selectivity and demonstrate the power of chemical exchange NMR to detect transient intermediates. Ultimately, we aim to build a catalogue of kinetic parameters allowing for the understanding and the eventual prediction of glycosylation reactions. We expect this technique to be applicable to various other types of glycosylation reaction intermediates such as additives (e.g. DMF, PPh₃O) and coordinating solvents (e.g. Et₂O, ACN). Finally, the application of the workflow laid out herein should be applicable to other types of reactions that are under Curtin-Hammett control.

Acknowledgements.

We thank Pepijn Geutjes, dr. Tom Bloemberg, and Luuk van Summeren from the Radboud University Faculty of Science teaching labs for allowing us to use their Bruker 300 MHz Avance III HD nanobay NMR spectrometer for conducting this research. Additionally, we would like to thank Luuk van Summeren for helping with the synthesis of 4-methoxy-[α -¹³C]-benzoic acid. We would also like to thank Dr. Adolfo Botana from the JEOL UK applications group for providing the CEST and modified EXSY pulse sequences and assisting in their implementation. This work was supported by a Dutch Research Council NWO-VIDI grant (VI.Vidi.192.070) awarded to T.J.B.

References.

- 1 Boltje, T. J., Buskas, T. & Boons, G.-J. Opportunities and challenges in synthetic oligosaccharide and glycoconjugate research. *Nature chemistry* **1**, 611-622 (2009).
- 2 Lemieux, R. U. Some implications in carbohydrate chemistry of theories relating to the mechanisms of replacement reactions. *Adv Carbohydr Chem* **9**, 1-57, doi:10.1016/s0096-5332(08)60371-9 (1954).
- 3 Frush, H. L. & Isbell, H. S. Sugar acetates, acetylglycosyl halides and orthoacetates in relation to the Walden inversion. *Journal of research of the National Bureau of Standards* **27**, 413 (1941).
- 4 Hettikankanamalage, A. A., Lassfolk, R., Ekholm, F. S., Leino, R. & Crich, D. Mechanisms of Stereodirecting Participation and Ester Migration from Near and Far in Glycosylation and Related Reactions. *Chemical Reviews* **120**, 7104-7151, doi:10.1021/acs.chemrev.0c00243 (2020).
- 5 Crich, D., Hu, T. & Cai, F. Does neighboring group participation by non-vicinal esters play a role in glycosylation reactions? Effective probes for the detection of bridging intermediates. *The Journal of organic chemistry* **73**, 8942-8953 (2008).
- 6 Baek, J. Y., Lee, B.-Y., Jo, M. G. & Kim, K. S. β -Directing Effect of Electron-Withdrawing Groups at O-3, O-4, and O-6 Positions and α -Directing Effect by Remote Participation of 3-O-Acyl and 6-O-Acetyl Groups of Donors in Mannopyranosylations. *Journal of the American Chemical Society* **131**, 17705-17713, doi:10.1021/ja907252u (2009).
- 7 Lei, J.-C., Ruan, Y.-X., Luo, S. & Yang, J.-S. Stereodirecting Effect of C3-Ester Groups on the Glycosylation Stereochemistry of L-Rhamnopyranose Thioglycoside Donors: Stereoselective Synthesis of α - and β -L-Rhamnopyranosides. *European Journal of Organic Chemistry* **2019**, 6377-6382, doi:https://doi.org/10.1002/ejoc.201901186 (2019).
- 8 Demchenko, A. V., Rousson, E. & Boons, G.-J. Stereoselective 1,2-cis-galactosylation assisted by remote neighboring group participation and solvent effects. *Tetrahedron Letters* **40**, 6523-6526, doi:https://doi.org/10.1016/S0040-4039(99)01203-4 (1999).
- 9 Baek, J. Y. *et al.* Directing effect by remote electron-withdrawing protecting groups at O-3 or O-4 position of donors in glycosylations and galactosylations. *Tetrahedron* **71**, 5315-5320, doi:https://doi.org/10.1016/j.tet.2015.06.014 (2015).
- 10 Ayala, L., Lucero, C. G., Romero, J. A., Tabacco, S. A. & Woerpel, K. A. Stereochemistry of nucleophilic substitution reactions depending upon substituent: evidence for electrostatic stabilization of pseudoaxial conformers of oxocarbenium ions by heteroatom substituents. *J Am Chem Soc* **125**, 15521-15528, doi:10.1021/ja037935a (2003).

- 11 Ma, Y., Lian, G., Li, Y. & Yu, B. Identification of 3,6-di-O-acetyl-1,2,4-O-orthoacetyl- α -D-glucopyranose as a direct evidence for the 4-O-acyl group participation in glycosylation. *Chemical Communications* **47**, 7515-7517, doi:10.1039/C1CC11680K (2011).
- 12 Komarova, B. S., Orekhova, M. V., Tsvetkov, Y. E. & Nifantiev, N. E. Is an acyl group at O-3 in glucosyl donors able to control α -stereoselectivity of glycosylation? The role of conformational mobility and the protecting group at O-6. *Carbohydr Res* **384**, 70-86, doi:10.1016/j.carres.2013.11.016 (2014).
- 13 Dejter-Juszynski, M. & Flowers, H. M. Studies on the koenigs-knorr reaction: Part IV: The effect of participating groups on the stereochemistry of disaccharide formation. *Carbohydrate Research* **28**, 61-74, doi:https://doi.org/10.1016/S0008-6215(00)82857-8 (1973).
- 14 McMillan, T. F. & Crich, D. Influence of 3-Thio Substituents on Benzylidene-Directed Mannosylation. Isolation of a Bridged Pyridinium Ion and Effects of 3-O-Picolyl and 3-S-Picolyl Esters. *European Journal of Organic Chemistry* **2022**, e202200320, doi:https://doi.org/10.1002/ejoc.202200320 (2022).
- 15 Elferink, H. *et al.* Competing C-4 and C-5-Acyl Stabilization of Uronic Acid Glycosyl Cations. *Chemistry – A European Journal* **28**, e202201724, doi:https://doi.org/10.1002/chem.202201724 (2022).
- 16 Remmerswaal, W. A. *et al.* Stabilization of Glucosyl Dioxolenium Ions by "Dual Participation" of the 2,2-Dimethyl-2-(ortho-nitrophenyl)acetyl (DMNPA) Protection Group for 1,2-cis-Glycosylation. *The Journal of Organic Chemistry* **87**, 9139-9147, doi:10.1021/acs.joc.2c00808 (2022).
- 17 de Kleijne, F. F. J., Elferink, H., Moons, S. J., White, P. B. & Boltje, T. J. Characterization of Mannosyl Dioxanion Ions in Solution Using Chemical Exchange Saturation Transfer NMR Spectroscopy. *Angewandte Chemie International Edition* **61**, e202109874, doi:https://doi.org/10.1002/anie.202109874 (2022).
- 18 Hansen, T. *et al.* Characterization of glycosyl dioxolenium ions and their role in glycosylation reactions. *Nature Communications* **11**, 2664, doi:10.1038/s41467-020-16362-x (2020).
- 19 Elferink, H. *et al.* The Glycosylation Mechanisms of 6,3-Uronic Acid Lactones. *Angewandte Chemie International Edition* **58**, 8746-8751, doi:https://doi.org/10.1002/anie.201902507 (2019).
- 20 Lemieux, R. U., Hendriks, K. B., Stick, R. V. & James, K. Halide ion catalyzed glycosidation reactions. Syntheses of α -linked disaccharides. *Journal of the American Chemical Society* **97**, 4056-4062, doi:10.1021/ja00847a032 (1975).
- 21 Lu, S.-R., Lai, Y.-H., Chen, J.-H., Liu, C.-Y. & Mong, K.-K. T. Dimethylformamide: An Unusual Glycosylation Modulator. *Angewandte Chemie International Edition* **50**, 7315-7320, doi:https://doi.org/10.1002/anie.201100076 (2011).
- 22 Crich, D. & Sun, S. Are Glycosyl Triflates Intermediates in the Sulfoxide Glycosylation Method? A Chemical and 1H, 13C, and 19F NMR Spectroscopic Investigation. *Journal of the American Chemical Society* **119**, 11217-11223, doi:10.1021/ja971239r (1997).
- 23 Santana, A. G. *et al.* Dissecting the Essential Role of Anomeric β -Triflates in Glycosylation Reactions. *Journal of the American Chemical Society* **142**, 12501-12514, doi:10.1021/jacs.0c05525 (2020).
- 24 Crich, D. & Chandrasekera, N. S. Mechanism of 4,6-O-Benzylidene-Directed β -Mannosylation as Determined by α -Deuterium Kinetic Isotope Effects. *Angewandte Chemie International Edition* **43**, 5386-5389, doi:https://doi.org/10.1002/anie.200453688 (2004).
- 25 Hansen, T. *et al.* Defining the SN1 Side of Glycosylation Reactions: Stereoselectivity of Glycopyranosyl Cations. *ACS Central Science* **5**, 781-788, doi:10.1021/acscentsci.9b00042 (2019).
- 26 Franconetti, A. *et al.* Glycosyl Oxocarbenium Ions: Structure, Conformation, Reactivity, and Interactions. *Accounts of Chemical Research* **54**, 2552-2564, doi:10.1021/acs.accounts.1c00021 (2021).
- 27 Huang, M., Retailleau, P., Bohé, L. & Crich, D. Cation Clock Permits Distinction Between the Mechanisms of α - and β -O- and β -C-Glycosylation in the Mannopyranose Series: Evidence for the Existence of a Mannopyranosyl Oxocarbenium Ion. *Journal of the American Chemical Society* **134**, 14746-14749, doi:10.1021/ja307266n (2012).

- 28 Chatterjee, S., Moon, S., Hentschel, F., Gilmore, K. & Seeberger, P. H. An Empirical Understanding of the Glycosylation Reaction. *Journal of the American Chemical Society* **140**, 11942-11953, doi:10.1021/jacs.8b04525 (2018).
- 29 Satoh, H., Hansen, H. S., Manabe, S., van Gunsteren, W. F. & Hünenberger, P. H. Theoretical Investigation of Solvent Effects on Glycosylation Reactions: Stereoselectivity Controlled by Preferential Conformations of the Intermediate Oxacarbenium-Counterion Complex. *Journal of Chemical Theory and Computation* **6**, 1783-1797, doi:10.1021/ct1001347 (2010).
- 30 Crich, D. & Cai, W. Chemistry of 4,6-O-Benzylidene-d-glycopyranosyl Triflates: Contrasting Behavior between the Gluco and Manno Series. *The Journal of Organic Chemistry* **64**, 4926-4930, doi:10.1021/jo990243d (1999).
- 31 van der Vorm, S. *et al.* Acceptor reactivity in glycosylation reactions. *Chemical Society Reviews* **48**, 4688-4706, doi:10.1039/C8CS00369F (2019).
- 32 Crich, D. En route to the transformation of glycoscience: A chemist's perspective on internal and external crossroads in glycochemistry. *Journal of the American Chemical Society* **143**, 17-34 (2020).
- 33 Adero, P. O., Amarasekara, H., Wen, P., Bohé, L. & Crich, D. The Experimental Evidence in Support of Glycosylation Mechanisms at the S(N)1-S(N)2 Interface. *Chem Rev* **118**, 8242-8284, doi:10.1021/acs.chemrev.8b00083 (2018).
- 34 Frihed, T. G., Bols, M. & Pedersen, C. M. Mechanisms of glycosylation reactions studied by low-temperature nuclear magnetic resonance. *Chemical reviews* **115**, 4963-5013 (2015).
- 35 Braak, F. t. *et al.* Characterization of Elusive Reaction Intermediates Using Infrared Ion Spectroscopy: Application to the Experimental Characterization of Glycosyl Cations. *Accounts of Chemical Research*, 6034-6038 (2022).
- 36 Elferink, H. *et al.* Direct Experimental Characterization of Glycosyl Cations by Infrared Ion Spectroscopy. *Journal of the American Chemical Society* **140**, 6034-6038, doi:10.1021/jacs.8b01236 (2018).
- 37 Mucha, E. *et al.* Unravelling the structure of glycosyl cations via cold-ion infrared spectroscopy. *Nature Communications* **9**, 4174, doi:10.1038/s41467-018-06764-3 (2018).
- 38 Martin, A. *et al.* Catching elusive glycosyl cations in a condensed phase with HF/SbF₅ superacid. *Nat Chem* **8**, 186-191, doi:10.1038/nchem.2399 (2016).
- 39 Crich, D. Mechanism of a Chemical Glycosylation Reaction. *Accounts of Chemical Research* **43**, 1144-1153, doi:10.1021/ar100035r (2010).
- 40 Aubry, S., Sasaki, K., Sharma, I. & Crich, D. Influence of protecting groups on the reactivity and selectivity of glycosylation: chemistry of the 4,6-o-benzylidene protected mannopyranosyl donors and related species. *Top Curr Chem* **301**, 141-188, doi:10.1007/128_2010_102 (2011).
- 41 D'Angelo, K. A. & Taylor, M. S. Borinic Acid Catalyzed Stereo- and Regioselective Couplings of Glycosyl Methanesulfonates. *Journal of the American Chemical Society* **138**, 11058-11066, doi:10.1021/jacs.6b06943 (2016).
- 42 Kahne, D., Walker, S., Cheng, Y. & Van Engen, D. Glycosylation of unreactive substrates. *Journal of the American Chemical Society* **111**, 6881-6882, doi:10.1021/ja00199a081 (1989).
- 43 Fraser-Reid, B., Wu, Z., Andrews, C. W., Skowronski, E. & Bowen, J. P. Torsional effects in glycoside reactivity: saccharide couplings mediated by acetal protecting groups. *Journal of the American Chemical Society* **113**, 1434-1435, doi:10.1021/ja00004a066 (1991).
- 44 Andrews, C. W., Rodebaugh, R. & Fraser-Reid, B. A Solvation-Assisted Model for Estimating Anomeric Reactivity. Predicted versus Observed Trends in Hydrolysis of n-Pentenyl Glycosides¹. *The Journal of Organic Chemistry* **61**, 5280-5289, doi:10.1021/jo9601223 (1996).
- 45 Jensen, H. H., Nordstrøm, L. U. & Bols, M. The Disarming Effect of the 4,6-Acetal Group on Glycoside Reactivity: Torsional or Electronic? *Journal of the American Chemical Society* **126**, 9205-9213, doi:10.1021/ja047578j (2004).
- 46 van Zijl, P. C. & Yadav, N. N. Chemical exchange saturation transfer (CEST): what is in a name and what isn't? *Magn Reson Med* **65**, 927-948, doi:10.1002/mrm.22761 (2011).
- 47 Lokesh, N., Seegerer, A., Hioe, J. & Gschwind, R. M. Chemical Exchange Saturation Transfer in Chemical Reactions: A Mechanistic Tool for NMR Detection and Characterization of Transient Intermediates. *Journal of the American Chemical Society* **140**, 1855-1862, doi:10.1021/jacs.7b12343 (2018).
- 48 Serianni, A. S., Pierce, J., Huang, S. G. & Barker, R. Anomerization of furanose sugars: kinetics of ring-opening reactions by proton and carbon-13 saturation-transfer NMR spectroscopy. *Journal of the American Chemical Society* **104**, 4037-4044, doi:10.1021/ja00379a001 (1982).
- 49 Woods, M., Woessner, D. E. & Sherry, A. D. Paramagnetic lanthanide complexes as PARACEST agents for medical imaging. *Chemical Society Reviews* **35**, 500-511, doi:10.1039/B509907M (2006).
- 50 Walvoort, M. T. C. *et al.* Equatorial Anomeric Triflates from Mannuronic Acid Esters. *Journal of the American Chemical Society* **131**, 12080-12081, doi:10.1021/ja905008p (2009).
- 51 Bock, K. & Pedersen, C. A study of ¹³CH coupling constants in hexopyranoses. *Journal of the Chemical Society, Perkin Transactions 2*, 293-297, doi:10.1039/P29740000293 (1974).
- 52 Crich, D., Cai, W. & Dai, Z. Highly Diastereoselective α -Mannopyranosylation in the Absence of Participating Protecting Groups. *The Journal of Organic Chemistry* **65**, 1291-1297, doi:10.1021/jo9910482 (2000).